

A Novel Cell-Based Multiplex Immunoassay Platform

Garnett Kelsoe (✉ garnett.kelsoe@duke.edu)

Duke University School of Medicine

Shengli Song

Duke University School of Medicine

Miriam Manook

Duke University School of Medicine

Jean Kwun

Duke University School of Medicine <https://orcid.org/0000-0002-8563-5472>

Annette Jackson

Duke University School of Medicine

Stuart Knechtle

Duke University School of Medicine <https://orcid.org/0000-0002-1625-385X>

Article

Keywords: Fluorescence Barcoding, Antibody to Membrane Proteins, Flow Cytometry Deconvolution, Immunity Characterization

Posted Date: May 21st, 2021

DOI: <https://doi.org/10.21203/rs.3.rs-464450/v1>

License:  This work is licensed under a Creative Commons Attribution 4.0 International License.

[Read Full License](#)

Version of Record: A version of this preprint was published at Communications Biology on November 25th, 2021. See the published version at <https://doi.org/10.1038/s42003-021-02881-w>.

1 **A Novel Cell-Based Multiplex Immunoassay Platform**

2

3 Shengli Song¹, Miriam Manook², Jean Kwun², Annette M. Jackson^{1,2}, Stuart J. Knechtle² and
4 Garnett Kelsoe^{1,2,*}

5 Departments of Immunology¹ and Surgery², Duke University School of Medicine, Durham, North
6 Carolina, USA

7 * Corresponding author, email: garnett.kelsoe@duke.edu

8

9 **Abstract**

10 We describe generation of stable, fluorescence-barcoded cell lines suitable for multiplex
11 screening of antibody to membrane proteins. The utility of this cell-based system, capable of a
12 256-plex cell panel, is demonstrated by flow cytometry deconvolution of barcoded cell panels
13 expressing influenza A hemagglutinin trimers, or native human CCR2 or CCR5 multi-spanning
14 proteins and their epitope-defining mutants. This platform may prove useful for characterizing
15 immunity and discovering antibodies to membrane-associated proteins.

16

17 **Main**

18 Membrane proteins are often critical immunogens in humoral responses to infection and
19 physiologically significant in health and disease. They are, therefore, valuable targets in vaccine
20 design and therapeutic antibody development¹. For many multi-subunit or multi-pass
21 transmembrane proteins, the native conformation is preserved only when the protein is properly
22 expressed on the cell membrane². For this reason, cell-based binding assays using protein
23 antigens expressed on the cell-surface are widely used in antibody screening and
24 characterization³. A major limitation in these assays is that they are single-analyte, or singleplex
25 methods, and consequently time-consuming, sample-depleting and costly when used to screen
26 samples with high numbers (>10) of antigens. While multiplex immunoassays based on the
27 Luminex[®] technology are well established, only acellular antigens can be immobilized on
28 detection beads with this platform.

29 Here, we describe a cell-based, multiplex immunoassay to fill this technology gap. Briefly, a
30 basal cell line was engineered to express different combinations of fluorescent proteins (FPs)
31 that can be reliably detected and distinguished in different channels on flow cytometers. This
32 resulted in a panel of fluorescence-barcoded reporter cell lines analogous to barcoded
33 Luminex[®] beads. Individual reporter cell sub-lines, each bearing a unique combination of FPs,
34 were subsequently engineered to express different cell-surface proteins to permit their pooling
35 in a cell-based multiplex immunoassay. Flow cytometry was then used to de-multiplex signals
36 from pooled reporter cell lines by serial gating for the identifying FP combinations. In this proof-
37 of-concept study, we established a 16-plex basic panel and tested the feasibility of expanding to
38 a 256-plex panel of reporter cell lines. We successfully applied this novel platform to multiplex
39 detection of antibody binding to cell panels expressing various influenza A hemagglutinin (HA)
40 trimers, or human CCR2b and CCR5 and several domain-swap or point mutants that define
41 specific protein domains/epitopes.

42 The human chronic myelogenous leukemia cell line K562 was selected as a parental cell line;
43 as a suspension cell line, detachment or digestion treatment is unnecessary, removing the
44 possibility of denaturation of expressed surface antigens. K562 cells also exhibit a high
45 efficiency of transfection and transduction, and are resilient to apoptosis⁴, simplifying the
46 processes of genetic modification and assay processing. A drawback of K562 as a reporter cell
47 line is its expression of the Fcγ receptor, CD32A, which binds most human IgG subclasses with
48 sufficient affinity to raise background thresholds (Supplementary Fig. 1). We therefore knocked-
49 out *CD32A* by CRISPR-Cas9 mediated gene targeting (Supplementary Fig. 1). Using genomic

50 DNA sequencing to ensure disabling all *CD32A* alleles, we generated a cloned, basal cell line,
51 K530. Compared with the parental K562 cells, K530 cells are negative for all Fcγ receptors
52 CD16, CD32, and CD64 and show minimal non-specific binding by human IgG1
53 (Supplementary Fig. 1).

54 To introduce unique barcodes into the reporter cells for multiplex detection, we conceived a
55 strategy to use combinations of FPs expressed in the cytosol of reporter cells. The growing
56 toolbox of FPs⁵ coupled with widely used multicolor flow cytometry allows for marking and
57 detecting multiple FPs simultaneously. The number of unique FP combinations is 2^n where n is
58 the number of different FPs. This exponential result provides the “power” for multiplexity. After
59 careful selection and experimental tests, we selected eight FPs (EBFP2⁶, mTurquoise2⁷,
60 mNeonGreen⁸, mCardinal⁹, mKate2¹⁰, miRFP703¹¹, LSSmOrange¹² and hmKeima8.5¹³;
61 Supplementary Table 1) with features including: 1) bright fluorescence for good separation and
62 limited spill-over into other fluorescence channels, 2) good photostability and low cytotoxicity,
63 and 3) monomeric FPs to avoid potential FRET events between heterologous FPs. We
64 designed and generated a four-color basic panel (Supplementary Fig. 2,3) capable of 16 distinct
65 FP combinations. Extended panels with two (Supplementary Fig. 2) or four additional colors
66 (Supplementary Fig. 3) could expand the multiplexity to 64- or 256-plex, respectively.
67 Alternatively, increased multiplexity could be achieved by introduction of a reference membrane
68 protein (*e.g.*, CD8a) or by high/low intensity versions of the same FPs (Supplementary Fig. 4).

69 We validated the four-color basic panel in supporting 16-plex detection of cell-surface
70 molecules. K530 cells were engineered to express all 16 combinations of four FPs from the
71 basic panel, resulting in 16 uniquely fluorescence-barcoded cell lines (Fig. 1a). Pooled cell lines
72 can be demultiplexed by flow cytometry based on patterns of FP expression (Fig. 1b). To
73 validate the deconvolution of multiplexed cell populations, we generated 16 cell lines expressing
74 human CD4, CD8a, CD86, or CD154 so that each protein was associated with four unique FP
75 patterns. The pooled cells were stained in single tubes with monoclonal antibody for one of the
76 four human antigens, followed by a common PE-conjugated secondary antibody. Deconvolution
77 by flow cytometry showed high resolution of bound and unbound cells and patterns of binding
78 consistent with antigen expression by barcoded cells before multiplexing (Fig. 1c,
79 Supplementary Fig. 5).

80 Influenza hemagglutinins (HAs) are diverse trimeric membrane proteins. Recombinant HA
81 protein preparation can be challenging as some HA ectodomains are unstable, and cell-surface
82 expression can be a surer option for obtaining native structure when working with unknown or
83 novel influenza strains. Multiplex immunoassays with collections of cell-surface expressed HA
84 antigens may be useful in influenza vaccine design and immunological monitoring. To
85 demonstrate, we prepared a panel of 12 reporter cell lines expressing the HA trimers of diverse
86 influenza A subtypes and successfully validated their structural integrity with several reference
87 antibodies (Supplementary Fig. 6). The pan-influenza A stem-binding antibody FI6¹⁴ bound to all
88 the HA antigens tested. The S5V2-29 antibody specific for a conserved interface epitope¹⁵
89 bound to a majority of group 1 and group 2 HAs tested and CH67, a neutralizing antibody for
90 H1N1 influenza¹⁶ bound HA from A/Solomon Islands/3/2006(H1N1) but not

91 A/Christchurch/16/2010(H1N1), an A/California/07/2009(H1N1)-like strain. Antibody HC19,
92 specific for HA A/Hong Kong/JY2/1968(H3N2)¹⁷ bound to that HA but not to others. We have
93 also successfully applied this assay in high-throughput screening of immunogen-specific
94 antibodies with single memory B cell cultures from influenza-vaccinated subjects (unpublished).

95 G protein-coupled receptors (GPCRs) are key to many biological functions and are an important
96 class of drug targets, contributing 34% of FDA approvals¹⁸. For these seven-pass
97 transmembrane proteins, mammalian cell surface expression is the most reliable way to
98 preserve native conformation. Domain/epitope mapping of GPCR-specific antibodies can be
99 helpful for structure-function studies of the receptors and for the screening antibodies for
100 therapeutic, diagnostic, and research applications¹⁹. A cell-based multiplex immunoassay that
101 could accommodate the large number of protein variants needed for domain/epitope mapping in
102 a single-tube could be useful. As an example, a panel of reporter cell lines was prepared,
103 expressing human CCR2b and CCR5 and 12 domain-swapped chimeric mutants (Fig. 2a). Two
104 CCR2-specific and five CCR5-specific antibodies were tested for their binding patterns to these
105 domain-swapped mutants in a multiplex immunoassay (Fig. 2b). We found the two
106 uncharacterized CCR2 antibodies to be specific for the CCR2 N1 domain (Fig. 2b,c). Of the
107 previously characterized CCR5 antibodies, CTC8, 2D7 and 45529 bound to the N1, ECL2A and
108 ECL2B domains, respectively, whereas binding of 45523 and 45549 was not isolated to any
109 single domain (Fig. 2b,c). These observations matched prior reports^{20,21}. The combination of
110 gain- and loss-of-binding readouts across all the ectodomains allowed a semi-quantitative
111 determination of the contribution of each individual ectodomain (Fig. 2c) and revealed more
112 minor-contributing domains unappreciated previously^{20,21}. Epitope mapping with another panel
113 of reporter cell lines expressing CCR5 mutants with alanine scanning (or glycine-to-serine
114 mutation) in ECL2A domain (Fig. 2d,e) showed that, consistent with previous studies^{20,21}, K171
115 and E172 were critically involved in the binding by 2D7 and 45523. With this scanning panel,
116 another five residues were also determined to be engaged in antibody binding, which were not
117 covered or appreciated in previous studies²⁰ is the
118 role of K171 and E172 in the binding by 45549 and awaits further confirmation. In practice, a full
119 scanning panel can be established to cover every residue in all ectodomains. This multiplex
120 immunoassay can enable high-throughput screening of antibodies with desired specificity and
121 potential function at single-residue resolution in a single-tube manner and expedite therapeutic
122 or diagnostic antibody discovery.

123 In summary, we have developed a cell-based multiplex immunoassay platform complementary
124 to the well-established Luminex[®] platform with acellular antigens. We validated its feasibility in
125 multiplexing and reliability in demultiplexing by flow cytometry. We demonstrated its broad
126 application in multiplex detection of antibody binding to influenza HA and domain/epitope
127 mapping against human CCR2b/CCR5 mutant antigens. The cell-based property of this platform
128 offers flexibility in multiplexing, superiority in supporting surface display of complex membrane
129 proteins in their native conformation, and economy in production once corresponding cell lines
130 are established. These unique features make this novel platform a valuable tool in humoral
131 response monitoring and antibody screening and characterization.

132 **Methods**

133 **Mice and human subjects**

134 Female C57BL/6 mice were obtained from the Jackson Laboratory and maintained under
135 specific-pathogen-free conditions at the Duke University Animal Care Facility. Splenocytes were
136 isolated from one 12-week-old mice for RNA extraction. All experiments involving animals were
137 approved by the Duke University Institutional Animal Care and Use Committee (IACUC A128-
138 20-06).

139 Peripheral blood mononuclear cells (PBMCs) were obtained from one human (*Homo sapiens*
140 *sapiens*) subject under Duke Institutional Review Board Committee guidelines (IRB
141 Pro00062495). Written informed consent was obtained.

142

143 **Original plasmids and DNA templates for gene cloning**

144 pU6-(BbsI)_CBh-Cas9-T2A-BFP (Addgene plasmid # 64323) was a gift from Ralf Kuehn²². pLV-
145 EF1a-IRES-Puro (Addgene plasmid # 85132) was a gift from Tobias Meyer²³. pLB (Addgene
146 plasmid # 11619) was a gift from Stephan Kissler²⁴. pMD2.G (Addgene plasmid # 12259) and
147 psPAX2 (Addgene plasmid # 12260) were gifts from Didier Trono. mScarlet-I-mTurquoise2
148 (Addgene plasmid # 98839) was a gift from Dorus Gadella²⁵. pLenti-smURFP-T2A-mCardinal
149 (Addgene plasmid # 80348) was a gift from Erik Rodriguez & Roger Tsien²⁶. pMito-miRFP703
150 (Addgene plasmid # 80000) was a gift from Vladislav Verkhusha¹¹. pLSSmOrange-mKate2
151 (Addgene plasmid # 99868) was a gift from Marc Tramier²⁷. Plasmid mNeonGreen-C1 was
152 provided by Allele Biotechnology and Pharmaceuticals Inc. under a license for non-commercial
153 use.

154 DNA template coding fluorescent protein (FP) hmKeima8.5 was synthesized (Genscript) based
155 on published amino acid sequences¹³. Coding sequences for other FPs were cloned from
156 plasmids mentioned above, with EBFP2⁶ from pU6-(BbsI)_CBh-Cas9-T2A-BFP, mTurquoise2⁷
157 from mScarlet-I-mTurquoise2, mNeonGreen⁸ from mNeonGreen-C1, mCardinal⁹ from pLenti-
158 smURFP-T2A-mCardinal, mKate2¹⁰ and LSSmOrange¹² from pLSSmOrange-mKate2 and
159 miRFP703¹¹ from pMito-miRFP703. Coding sequences for cytoplasmic domain truncated
160 mouse CD4 (amino acid (aa) 1-423), CD8a (aa 1-222) and CD86 (aa 1-268) were cloned from
161 splenocyte cDNA samples from one C57BL/6 mouse. Coding sequences for full length human
162 CCR2b and CCR5, and cytoplasmic domain truncated human CD4 (aa 1-424), CD8a (aa 1-
163 209), CD86 (aa 1-276) and CD154 (aa 1-240) were cloned from PBMC cDNA samples from one
164 healthy donor.

165 DNA templates coding influenza hemagglutinin (HA) antigens A/Christchurch/16/2010(H1N1)
166 (GISAID Accession EPI280344) and A/Texas/50/2012(H3N2) (GenBank Accession KJ942744)
167 were synthesized (Gene Universal Inc.) based on amino acid sequences in the databases.
168 Plasmid containing coding sequences for influenza HA A/Solomon Islands/3/2006(H1N1)
169 (GenBank EU100724, with R540L correction) was provided by Aaron G. Schmidt (Ragon
170 Institute). Plasmids containing coding sequences for other influenza HA antigens used were
171 provided by Stephen C. Harrison (Harvard Medical School), including HA antigens
172 A/Japan/305/1957(H2N2) (GenBank CY014976), A/Hong Kong/JY2/1968(H3N2) (GenBank
173 CY147438), A/American black duck/New Brunswick/00464/2010(H4N6) (GenBank CY138045),

174 A/Viet Nam/1203/2004(H5N1) (GenBank AY818135), A/Taiwan/2/2013(H6N1) (GISAID
175 EPI459855), A/Taiwan/1/2017(H7N9) (GISAID EPI917065), A/northern
176 shoveler/California/HKWF1204/2007(H8N4) (GenBank CY039588),
177 A/Jiangxi/IPB13/2013(H10N8) (GenBank KJ406543) and
178 A/mallard/Wisconsin/10OS3941/2010(H14N6) (GenBank CY133266).

179

180 **Plasmid modification and gene cloning**

181 Standard molecular cloning procedures were followed for plasmid modification and gene
182 cloning. Endotoxin-free plasmids were prepared (E.Z.N.A.[®] Endo-free Plasmid DNA Mini Kit II,
183 Omega Bio-tek) for mammalian cell transfection. Recombinant sequences in all plasmids used
184 were verified by DNA Sanger sequencing (The Duke University DNA Analysis Facility).

185 The empty lentiviral transfer vector plasmids pLB-EF1a, pLB-EFS and pLB-EF1a-IRES-Puro
186 (pLB-EXIP; IRES stands for internal ribosome entry site) were constructed by replacing the U6-
187 loxP-CMV-EGFP-loxP cassettes in plasmid pLB with EF1a promoter, EFS core promoter
188 (nucleotide 1-226 of EF1a promoter, with attenuated transcription activity) or EF1a-IRES-Puro
189 cassettes from plasmid pLV-EF1a-IRES-Puro, respectively. pLB-EXIP was further modified to
190 generate bicistronic vectors pLB-EF1a-IRES-EBFP2, pLB-EF1a-IRES-mTurquoise2, pLB-EF1a-
191 IRES-mCardinal, pLB-EF1a-IRES-mCD4, pLB-EF1a-IRES-mCD8a, pLB-EF1a-IRES-mCD86 by
192 replacing puromycin-resistant gene in pLB-EXIP with coding sequences for corresponding
193 genes following IRES element. pLB-EFS-IRES-mNeonGreen was generated from pLB-EXIP by
194 replacing EF1a promoter with EFS core promoter and puromycin-resistant gene with
195 mNeonGreen coding sequences.

196 Lentiviral transfer vector plasmids expressing EBFP2, mTurquoise2, mCardinal, mKate2,
197 miRFP703, LSSmOrange, hmKeima8.5 were generated by cloning of corresponding coding
198 sequences into pLB-EF1a. Lentiviral transfer vector plasmid expressing mNeonGreen was
199 generated by cloning of mNeonGreen coding sequences into pLB-EFS. Human CD4, CD8a,
200 CD86 and CD154 coding sequences (with cytoplasmic domain truncations, see above) were
201 cloned into pLB-EXIP for puromycin-mediated selection. Human CD8a coding sequences were
202 cloned into pLB-EF1a-IRES-mTurquoise2 and pLB-EF1a-IRES-mCardinal, and human CD86
203 coding sequences were cloned into pLB-EF1a-IRES-EBFP2 and pLB-EFS-IRES-mNeonGreen.
204 These bicistronic expression vectors can co-express human CD8a/CD86 and FPs, with FPs at a
205 lower expression level driven by IRES element. Coding sequences for influenza HA antigens,
206 human CCR2b, CCR5 and their domain-swapped or point mutants were cloned into pLB-EXIP.

207

208 **Culture, transfection and transduction of mammalian cell lines**

209 HEK 293T and K562 cell lines were purchased from ATCC. HEK 293T cells were cultured in
210 DMEM medium (Gibco) supplemented with 10% heat-inactivated HyClone FBS (Cytiva), 10 mM
211 HEPES buffer and 55 μ M 2-Mercaptoethanol (all Gibco). K562 and derivative cell lines were
212 maintained in RPMI-1640 medium (Gibco) supplemented with 10% heat-inactivated HyClone
213 FBS, 10 mM HEPES buffer, 1 mM sodium pyruvate, 1 \times MEM NEAA, 55 μ M 2-Mercaptoethanol,
214 100 units/ml penicillin and 100 μ g/ml streptomycin (all Gibco). For all K562 derivative cell lines,

215 monoclonal cell lines were established by single-cell sorting (see below) and used in binding
216 assays in this study.

217 Single-guide RNAs (sgRNAs) targeting human *CD32A* exon 1 were designed with the online
218 tool (<http://crispr.mit.edu>). sgRNAs used in this study were sgRNA-hCD32A-1
219 (AGCAGCAGCAAACACTGTCAA), sgRNA-hCD32A-2 (ATGTATGTCCCAGAAACCTG) and a
220 negative control sgRNA (TGTCATGCGTCACTTAGTGC). Corresponding DNA oligos were
221 synthesized and cloned into plasmid pU6-(BbsI)_CBh-Cas9-T2A-BFP. K562 cells were
222 transfected with CRISPR-Cas9 targeting plasmids using Lipofectamine 3000 Transfection
223 Reagent (Invitrogen). 96 hours after transfection, the cells were harvested for flow cytometry
224 analysis and single-cell sorting (see below).

225 Lentiviral transfer vector plasmids were co-transfected into HEK 293T cells with packaging
226 plasmids pMD2.G and psPAX2 using Lipofectamine 3000 Transfection Reagent (Invitrogen).
227 Forty-eight hours after transfection, culture supernatants were harvested and filtered through
228 0.45- μ m PVDF membrane filters (Millipore). K562 derivative cell lines were transduced with the
229 filtered supernatants containing lentiviral vectors by spinoculation at 1000 \times *g* for 45 min at 32°C.
230 For transductions with pLB-EXIP-based vectors, cells were selected with puromycin (Sigma, 2
231 μ g/ml) between 3-7 days after transduction. Seven days after transduction, the cells were
232 harvested for flow cytometry analysis and single-cell sorting (see below).

233

234 **Antibodies**

235 Monoclonal antibodies used in this study included: FITC-conjugated anti-human CD32A
236 (hCD32A-FITC, clone IV.3, STEMCELL 60012FI), hCD32-APC (clone FLI8.26, BD 559769),
237 hCD16-PE (clone 3G8, BioLegend 302007), hCD32-PE (clone FLI8.26, BD 550586), hCD64-PE
238 (clone 10.1, BioLegend 305007), hCD4 (clone SK3, BioLegend 344602), hCD8a (clone HIT8a,
239 BioLegend 300902), hCD86 (clone BU63, BioLegend 374202), hCD154 (clone 24-31,
240 BioLegend 310802), mCD8a-PerCP-eFluor710 (mouse CD8a, clone 53-6.7, ThermoFisher 46-
241 0081), mCD86-PE-Vio770 (clone PO3.3, Miltenyi Biotec 130-105-135), mCD4-APC-Fire750
242 (clone RM4-5, BioLegend 100568), hCD58-PE (clone MEM-63, ThermoFisher MA1-10256), HA
243 tag (clone 16B12, BioLegend 901533), hCCR2 (clone K036C2, BioLegend 357201), hCCR2
244 (clone 48607, R&D Systems MAB150), hCCR5 (clone 2D7, BD 555991), hCCR5 (clone CTC8,
245 R&D Systems MAB1801), hCCR5 (clone 45523, R&D Systems MAB181), hCCR5 (clone 45529,
246 R&D Systems MAB184), hCCR5 (clone 45549, R&D Systems MAB183). Isotype control
247 antibodies included: Mouse IgG1 Kappa isotype control (Rockland 010-001-330), Human IgG1
248 Kappa (hIgG1K, Southern Biotech 0151K-01), Human IgG1 Lambda (hIgG1L, Southern Biotech
249 0151L-01). Secondary antibodies included: Goat Anti-Human IgG-PE (Southern Biotech 2040-
250 09), Goat Anti-Mouse IgG, Human ads-PE (Southern Biotech 1030-09). Influenza hemagglutinin
251 specific antibodies FI6¹⁴, S5V2-29¹⁵, CH67¹⁶ and HC19¹⁷ were prepared as recombinant human
252 IgG1 antibodies as described²⁸.

253

254 **Cell surface staining, flow cytometry analysis and single-cell sorting and cloning**

255 Cultures of K562 and derivative cells were harvested, centrifuged at 300 \times *g* for 2 min at 4°C and
256 resuspended in staining buffer (PBS supplemented with 2% heat-inactivated FBS). After

257 incubation with antibodies at 4°C in the dark for 30 min, cells were washed with staining buffer
258 and resuspended in staining buffer for either secondary staining following the same procedure
259 above or stored on ice for flow cytometry analysis or single-cell sorting.

260 Flow cytometry analysis was carried out using either BD FACSCanto II cytometer (Duke Cancer
261 Institute Flow Cytometry Shared Resource) or BD LSR II cytometer (The Duke Human Vaccine
262 Institute (DHVI) Research Flow Cytometry Facility). Single-cell sorting was performed with BD
263 Aria II (The DHVI Research Flow Cytometry Facility). The bulk cell line after transfection or
264 transduction were stained with corresponding antibodies and single cells expressing FP or
265 antigen of interest were sorted into 96-well flat-bottom plates containing 100 µl/well of the
266 complete RPMI medium above supplemented with 20% heat-inactivated FBS. Nine days after
267 sorting, healthily proliferating cell clones were transferred into 24-well plates for further
268 expansion. Three days later, individual monoclonal cell lines were validated for the expression
269 of FP or antigen of interest and a single clone with a uniform expression level was selected for
270 further engineering or used as a reporter cell line in immunoassays.

271

272 **Data analysis**

273 FlowJO (Version 10.7.2), Chromas (Version 2.6.6) and Microsoft Office (Version 1808) were
274 used to analyze data and prepare figures for publication.

275

276 **Acknowledgements**

277 We thank Xiaoyan Nie, Dongmei Liao, Xiaoe Liang and Nikita Hall for technical assistance. The
278 research was supported by NIH grant R01 AI128832 (to G.K.).

279

280 **Author Contributions**

281 S.S. and G.K. conceived the project. S.S. and M.M. performed experiments. All authors
282 analyzed the data and prepared the manuscript.

283

284 **Competing Interests statement**

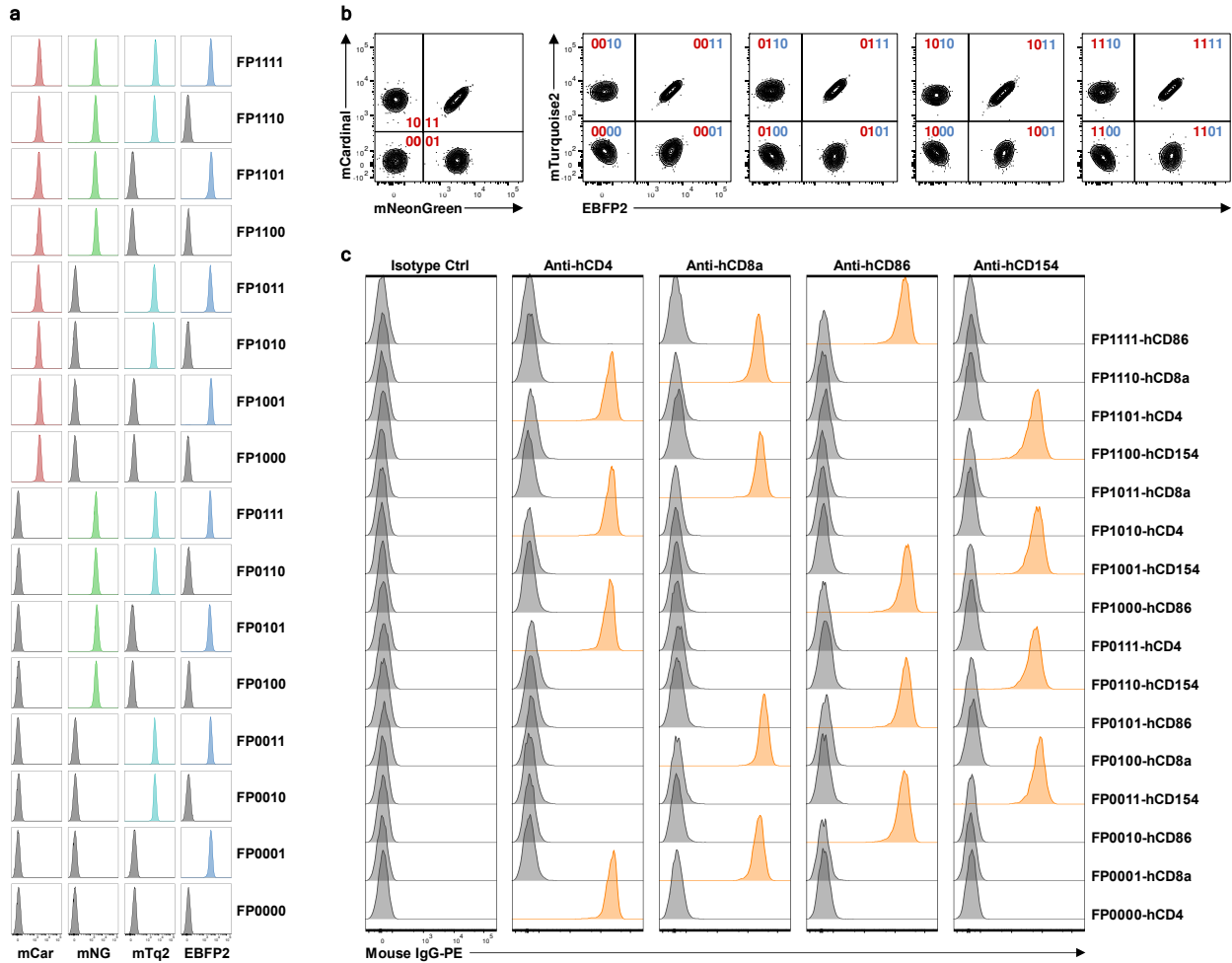
285 Our institution, Duke University, has a patent application related to this work. Names of
286 inventors are Shengli Song and Garnett Kelsoe. Application number is 63/033,444. Status of
287 application is patent pending. The patent application covered the design and application of the
288 novel cell-based immunoassay platform reported here.

289

290 **References**

- 291 1. Dodd, R.B., Wilkinson, T. & Schofield, D.J. Therapeutic Monoclonal Antibodies to
 292 Complex Membrane Protein Targets: Antigen Generation and Antibody Discovery
 293 Strategies. *BioDrugs* **32**, 339-355 (2018).
- 294 2. Cournia, Z. et al. Membrane Protein Structure, Function, and Dynamics: a Perspective
 295 from Experiments and Theory. *J Membr Biol* **248**, 611-640 (2015).
- 296 3. Alfaleh, M.A., Jones, M.L., Howard, C.B. & Mahler, S.M. Strategies for Selecting
 297 Membrane Protein-Specific Antibodies using Phage Display with Cell-Based Panning.
 298 *Antibodies (Basel)* **6** (2017).
- 299 4. McGahon, A.J. et al. Downregulation of Bcr-Abl in K562 cells restores susceptibility to
 300 apoptosis: characterization of the apoptotic death. *Cell Death Differ* **4**, 95-104 (1997).
- 301 5. Rodriguez, E.A. et al. The Growing and Glowing Toolbox of Fluorescent and Photoactive
 302 Proteins. *Trends Biochem Sci* **42**, 111-129 (2017).
- 303 6. Ai, H.W., Shaner, N.C., Cheng, Z., Tsien, R.Y. & Campbell, R.E. Exploration of new
 304 chromophore structures leads to the identification of improved blue fluorescent proteins.
 305 *Biochemistry* **46**, 5904-5910 (2007).
- 306 7. Goedhart, J. et al. Structure-guided evolution of cyan fluorescent proteins towards a
 307 quantum yield of 93%. *Nat Commun* **3**, 751 (2012).
- 308 8. Shaner, N.C. et al. A bright monomeric green fluorescent protein derived from
 309 *Branchiostoma lanceolatum*. *Nat Methods* **10**, 407-409 (2013).
- 310 9. Chu, J. et al. Non-invasive intravital imaging of cellular differentiation with a bright red-
 311 excitable fluorescent protein. *Nat Methods* **11**, 572-578 (2014).
- 312 10. Shcherbo, D. et al. Far-red fluorescent tags for protein imaging in living tissues. *Biochem*
 313 *J* **418**, 567-574 (2009).
- 314 11. Shcherbakova, D.M. et al. Bright monomeric near-infrared fluorescent proteins as tags
 315 and biosensors for multiscale imaging. *Nat Commun* **7**, 12405 (2016).
- 316 12. Shcherbakova, D.M., Hink, M.A., Joosen, L., Gadella, T.W. & Verkhusha, V.V. An
 317 orange fluorescent protein with a large Stokes shift for single-excitation multicolor FCCS
 318 and FRET imaging. *J Am Chem Soc* **134**, 7913-7923 (2012).
- 319 13. Guan, Y. et al. Live-cell multiphoton fluorescence correlation spectroscopy with an
 320 improved large Stokes shift fluorescent protein. *Mol Biol Cell* **26**, 2054-2066 (2015).
- 321 14. Corti, D. et al. A neutralizing antibody selected from plasma cells that binds to group 1
 322 and group 2 influenza A hemagglutinins. *Science* **333**, 850-856 (2011).
- 323 15. Watanabe, A. et al. Antibodies to a Conserved Influenza Head Interface Epitope Protect
 324 by an IgG Subtype-Dependent Mechanism. *Cell* **177**, 1124-1135 e1116 (2019).
- 325 16. Whittle, J.R. et al. Broadly neutralizing human antibody that recognizes the receptor-
 326 binding pocket of influenza virus hemagglutinin. *Proc Natl Acad Sci U S A* **108**, 14216-
 327 14221 (2011).
- 328 17. Bizebard, T. et al. Refined three-dimensional structure of the Fab fragment of a murine
 329 IgG1,lambda antibody. *Acta Crystallogr D Biol Crystallogr* **50**, 768-777 (1994).
- 330 18. Hauser, A.S., Attwood, M.M., Rask-Andersen, M., Schioth, H.B. & Gloriam, D.E. Trends
 331 in GPCR drug discovery: new agents, targets and indications. *Nat Rev Drug Discov* **16**,
 332 829-842 (2017).
- 333 19. Hutchings, C.J. A review of antibody-based therapeutics targeting G protein-coupled
 334 receptors: an update. *Expert Opin Biol Ther*, 1-11 (2020).
- 335 20. Lee, B. et al. Epitope mapping of CCR5 reveals multiple conformational states and
 336 distinct but overlapping structures involved in chemokine and coreceptor function. *J Biol*
 337 *Chem* **274**, 9617-9626 (1999).
- 338 21. Paes, C. et al. Atomic-level mapping of antibody epitopes on a GPCR. *J Am Chem Soc*
 339 **131**, 6952-6954 (2009).

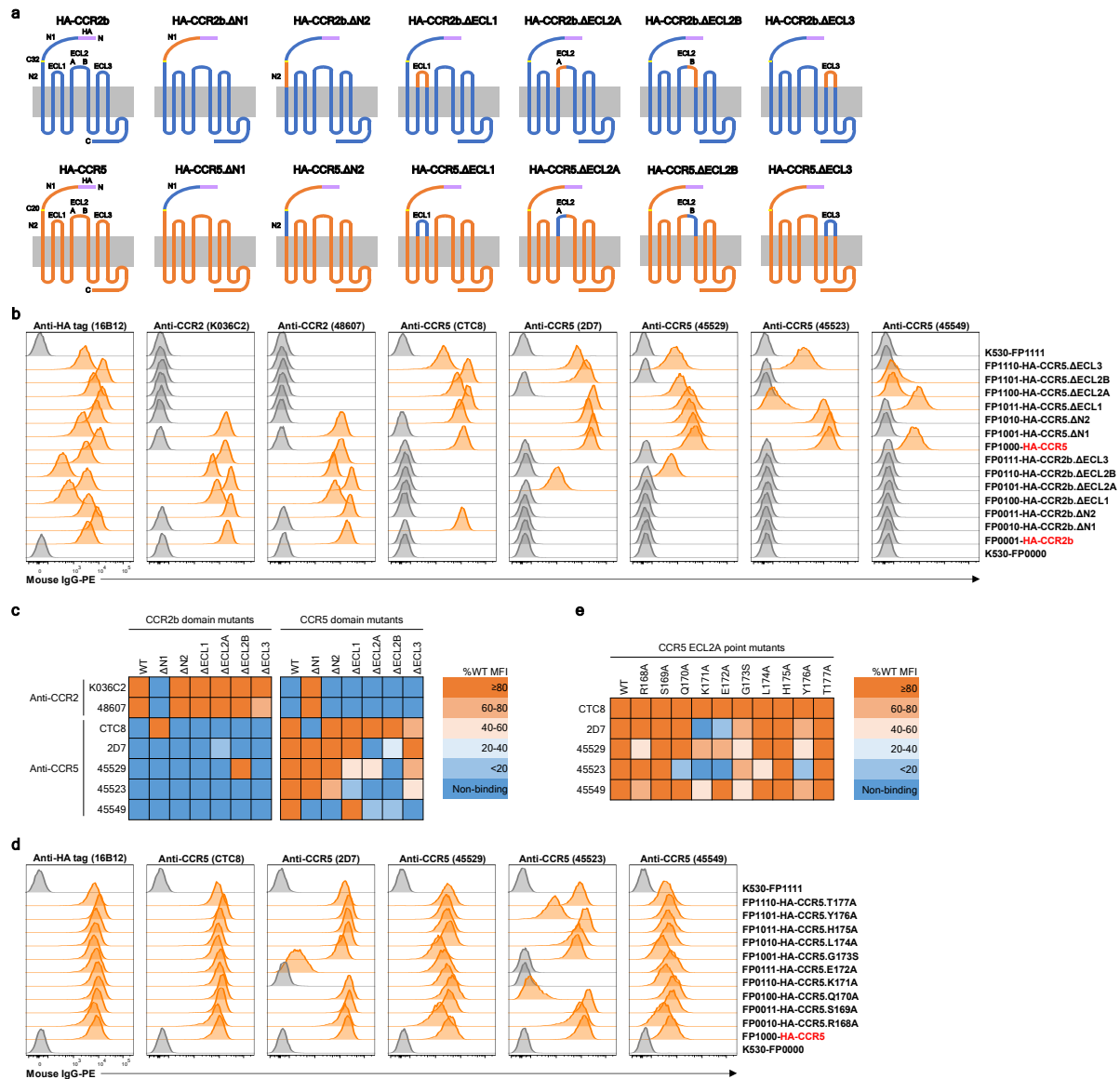
340 22. Chu, V.T. et al. Increasing the efficiency of homology-directed repair for CRISPR-Cas9-
341 induced precise gene editing in mammalian cells. *Nat Biotechnol* **33**, 543-548 (2015).
342 23. Hayer, A. et al. Engulfed cadherin fingers are polarized junctional structures between
343 collectively migrating endothelial cells. *Nat Cell Biol* **18**, 1311-1323 (2016).
344 24. Kissler, S. et al. In vivo RNA interference demonstrates a role for Nramp1 in modifying
345 susceptibility to type 1 diabetes. *Nat Genet* **38**, 479-483 (2006).
346 25. Mastop, M. et al. Characterization of a spectrally diverse set of fluorescent proteins as
347 FRET acceptors for mTurquoise2. *Sci Rep* **7**, 11999 (2017).
348 26. Rodriguez, E.A. et al. A far-red fluorescent protein evolved from a cyanobacterial
349 phycobiliprotein. *Nat Methods* **13**, 763-769 (2016).
350 27. Demeautis, C. et al. Multiplexing PKA and ERK1&2 kinases FRET biosensors in living
351 cells using single excitation wavelength dual colour FLIM. *Sci Rep* **7**, 41026 (2017).
352 28. Tiller, T. et al. Efficient generation of monoclonal antibodies from single human B cells
353 by single cell RT-PCR and expression vector cloning. *J Immunol Methods* **329**, 112-124
354 (2008).
355
356



357

358 **Figure 1. A multiplex immunoassay based on fluorescence-barcoded reporter cell lines. a,**
 359 **A basic panel of fluorescence-barcoded reporter cell lines. K530 cells were transduced with**
 360 **different combinations of four FPs to produce 16 uniquely fluorescence-barcoded cell lines. The**
 361 **absence/presence of fluorescence from FPs EBFP2, mTurquoise2 (mTq2), mNeonGreen (mNG)**
 362 **and mCardinal (mCar) are designated as four digits of binary barcodes as shown on the right of**
 363 **histograms for each individual cell line. b, Demultiplexing of pooled fluorescence-barcoded**
 364 **reporter cell lines by flow cytometry. c, The 16 barcoded reporter cell lines were transduced to**
 365 **express human CD4, CD8a, CD86 and CD154 molecules in a shifted pattern relative to FP**
 366 **expression. These cells were pooled and stained with corresponding mouse monoclonal**
 367 **antibodies (as indicated on the top of each histogram) followed by a PE-conjugated anti-mouse**
 368 **IgG antibody. Signals from individual reporter cell lines were demultiplexed as shown in b, and**
 369 **the binding by corresponding antibodies were plotted as half-offset histograms. In all cases, the**
 370 **detected expression patterns were consistent with antigen expression by barcoded cells before**
 371 **multiplexing as shown on the right of histograms for each individual cell line. Isotype Ctrl, mouse**
 372 **IgG1, kappa isotype control antibody.**

373



374

375 **Figure 2. Application of the multiplex immunoassay in domain/epitope mapping of**
 376 **antibodies specific for human CCR2 and CCR5.** **a**, Schematic diagrams showing CCR2b and
 377 CCR5 domain-swapped mutants expressed on reporter cell lines. An N-terminal HA-tag was
 378 included to normalize surface expression levels of different mutants. **b**, Domain mapping with
 379 multiplexed reporter cell lines expressing CCR2b and CCR5 domain-swapped mutants. The
 380 binding to each reporter cell line was demultiplexed as shown in Figure 1. Histograms with MFI
 381 values above 2-fold of background (the average MFI value of internal control cell lines K530-
 382 FP0000 and K530-FP1111) were scored as positive and highlighted in orange. **c**, Heat map of
 383 the relative binding activities of antibodies tested in **b**. Background-subtracted MFI values were
 384 first normalized to that with anti-HA-tag antibody and then to corresponding cell lines expressing
 385 WT molecules. Percentages of WT MFI values were color-coded according to the key. Negative
 386 readouts in **b** were indicated as non-binding. **d**, Epitope mapping with multiplexed reporter cell
 387 lines expressing CCR5 ECL2A point mutants. The data were analyzed in the same way as in **b**.
 388 **e**, Heat map of the relative binding activities of antibodies tested in **d** and plotted in the same
 389 way as in **c**. All monoclonal mouse antibodies were used at 5 µg/ml.

Supplementary Files

This is a list of supplementary files associated with this preprint. Click to download.

- [Supplementary.pdf](#)